

Ante, Mirko; Sörgel, Şeniz; Opitz, Martin; Freudenberger, Renate; Bund, Andreas:

**Electrocatalysis of lithium (poly-) sulfides in organic ether-based electrolytes**

---

*Original published in:* Journal of the Electrochemical Society / Electrochemical Societyristol : IOP Publishing. - 167 (2021), 16, art. 166520, 9 pp.

*Original published:* 2021-01-04

*ISSN:* 1945-7111

*DOI:* [10.1149/1945-7111/abd60c](https://doi.org/10.1149/1945-7111/abd60c)

*[Visited:* 2021-06-07]



This work is licensed under a [Creative Commons Attribution 4.0 International license](https://creativecommons.org/licenses/by/4.0/). To view a copy of this license, visit <https://creativecommons.org/licenses/by/4.0/>

---



# Electrocatalysis of Lithium (Poly-) Sulfides in Organic Ether-Based Electrolytes

M. J. Ante,<sup>1,2,\*</sup>  Ş. Sörgel,<sup>1</sup> M. Opitz,<sup>1</sup> R. Freudenberger,<sup>1</sup> and A. Bund<sup>2,\*\*</sup> 

<sup>1</sup>Department of Electrochemistry, Forschungsinstitut Edelmetalle + Metallchemie, 73525 Schwäbisch Gmünd, Germany

<sup>2</sup>Electrochemistry and Electroplating Group, Technische Universität Ilmenau, 98693 Ilmenau, Germany

This work aims at identifying an effective electrocatalyst for polysulfide reactions to improve the electrode kinetics of the sulfur half-cell in liquid organic electrolytes for alkali-sulfur cells. To increase the charge and discharge rates and energy efficiency of the cell, functionalized electrocatalytic coatings have been prepared and their electrode kinetics have been measured. To the best of our knowledge, there is no extensive screening of electrocatalysts for the sulfur electrode in dimethoxyethane:1,3-dioxolane (DME:DOL) electrolytes. In order to identify a suitable electrocatalyst, apparent exchange current densities at various materials (Al, Co, Cr, Cu, Fe, Steel, glassy carbon, ITO, Ni, Pt, Ti, TiN, Zn) are evaluated in a polysulfide electrolyte using potentiodynamic measurements with a Butler-Volmer fit. The chemical stability and surface morphology changes after electrochemical measurements are assessed with X-ray diffraction (XRD) and Scanning Electron Microscopy (SEM). The results show that cobalt is a promising candidate with appropriate electrocatalytic properties for polysulfide reactions while being stable in the electrochemical environment, followed by chromium in terms of catalytic activity and stability. Sputtered TiN was found to be a very stable material with very low catalytic activity, a possible current collector for the cell.

© 2021 The Author(s). Published on behalf of The Electrochemical Society by IOP Publishing Limited. This is an open access article distributed under the terms of the Creative Commons Attribution 4.0 License (CC BY, <http://creativecommons.org/licenses/by/4.0/>), which permits unrestricted reuse of the work in any medium, provided the original work is properly cited. [DOI: 10.1149/1945-7111/abd60c]



Manuscript submitted June 11, 2020; revised manuscript received December 11, 2020. Published January 4, 2021.

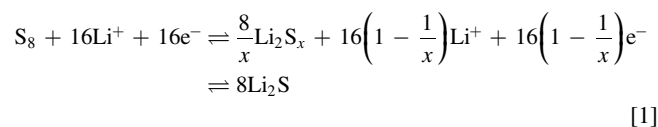
Supplementary material for this article is available [online](#)

**Lithium sulfur battery.**—Lithium-Sulfur (Li-S) battery systems theoretically provide high specific gravimetric and volumetric energy density (2600 Wh kg<sup>-1</sup> and 2800 Wh l<sup>-1</sup>).<sup>1,2</sup> Hence, Li-S batteries are promising candidates for mobile and stationary applications. Furthermore, the Li-S battery system is potentially low-cost<sup>1,3</sup> and environmentally benign<sup>1,3</sup> compared to other lithium battery systems. However, the technical implementation suffers from limited cycling stability, low charge and discharge rates and deficiencies in the understanding of the complex polysulfide reaction mechanism.<sup>4</sup>

**Polysulfide shuttle mechanism.**—During discharge, i.e. the reduction of S<sub>8</sub>, polysulfides with different chain lengths are formed<sup>5,6</sup> (Li<sub>2</sub>S<sub>x</sub>, 2 ≤ x ≤ 8). Some of these polysulfides are soluble (Li<sub>2</sub>S<sub>x</sub>, 4 ≤ x ≤ 8) in the typical Li-S battery electrolytes like glymes (ethylene glycol dimethyl ether, diethylene glycol dimethyl ether, triethylene glycol dimethyl ether or tetraethylene glycol dimethyl ether) or dimethoxyethane:1,3-dioxolane (DME:DOL).<sup>7</sup> Once dissolved, polysulfides diffuse to the negative electrode and react with the metallic lithium. The reaction products (Li<sub>2</sub>S<sub>2</sub> and Li<sub>2</sub>S) are insoluble and passivate the negative electrode.<sup>8</sup> Furthermore, the loss of sulfur from the positive electrode decreases the capacity of the battery. The most common approach to overcome the challenges of this shuttle mechanism is to tailor the sulfur containing electrode structure by trapping sulfur and polysulfides mainly in carbon based nanostructures.<sup>9-12</sup> In contrast the concept of this work is to minimize the shuttle mechanism by using an effective electrocatalyst for the polysulfide oxidation/reduction reactions. A fast and complete formation of Li<sub>2</sub>S at the positive electrode would minimize the formation of intermediate soluble species and thus maximize the cell capacity.

**Lithium sulfur electrocatalysis.**—Electrocatalysis is an important research field in many applications such as fuel cells,<sup>13,14</sup> batteries,<sup>15</sup> synthesis,<sup>16,17</sup> sensors<sup>18</sup> or waste water treatment.<sup>19</sup> Electrocatalysts for the sulfur electrode reaction (Eq. 1) are so far insufficiently studied although their understanding could help to

overcome the drawbacks of lithium sulfur batteries.



An important parameter for an electrocatalyst is the exchange current density,  $j_0$  (Eq. 2).<sup>11,12</sup> The driving forces for the anodic and the cathodic partial current densities are defined as  $e_a$  and  $e_c$  (Eq. 3).

$$j = j_0 (e_a - e_c) \quad [2]$$

$j$ —current density;  $j_0$ —exchange current density

$$e_a = \exp(b_a \eta); e_c = \exp(b_c \eta) \quad [3]$$

$a$ —anodic;  $c$ —cathodic;  $b$ —exponential coefficients for multi-electron reactions;  $\eta$ —overpotential.

Simply speaking, the higher the exchange current density, the higher is the electrocatalytic activity of a material for the corresponding electrode reaction.

At higher overpotentials, the current may be limited by the diffusion of the electro-active species. In this case, Butler-Volmer kinetics with diffusion limitation<sup>20,21</sup> can be applied (Eq. 4).

$$j = j_0 \left( \frac{c_{\text{red}}}{c_{\text{red}}^*} \cdot e_a - \frac{c_{\text{ox}}}{c_{\text{ox}}^*} \cdot e_c \right) \quad [4]$$

$c_{\text{red}}$ —concentration of the reduced species at the electrode surface;  $c_{\text{ox}}$ —concentration of the oxidized species at the electrode surface;  $c_{\text{red}}^*$ —bulk concentration of the reduced species;  $c_{\text{ox}}^*$ —bulk concentration of the oxidized species.

In case of the sulfur electrode, during charge and discharge, various electrochemical and chemical reactions of different polysulfides with chain lengths between Li<sub>2</sub>S and Li<sub>2</sub>S<sub>8</sub> occur, in the following referred to as Li<sub>2</sub>S<sub>x</sub>.<sup>22</sup> However, not all chain lengths are stable and therefore might not emerge during cycling of the battery (e.g.  $x = 3$ ,  $x = 5$  and  $x = 7$ ) The reaction intermediates with  $4 \leq x \leq 8$  are highly soluble in the electrolyte. The smaller di- and monosulfides ( $x \leq 2$ ) and sulfur (S<sub>8</sub>)

\*Electrochemical Society Student Member.

\*\*Electrochemical Society Member.

<sup>z</sup>E-mail: [Mirko.Ante@gmx.de](mailto:Mirko.Ante@gmx.de)

**Table I. Composition and purity of the screening candidates, that were used “as received” after pretreatment (GB: Glovebox, SS: Stainless Steel, GC: Glassy Carbon).**

Samples	Form	Supplier	Pre-treatment	Comment
Al	Foil	Alfa Aesar	scratch in GB	99.99% purity, 0.1 mm
Ni	Foil	Schlenk GmbH	Schlötter EL-KG	99.6% purity
Pt	Foil	C. Hafner	scratch in GB	>99.99% purity
GC	Disk	Belltech GmbH	scratch in GB	1.4305, contains Cr and Ni
SS	Plate	Varta Microbatteries	scratch in GB	99.95% purity, 0.001 in
Co	Foil	Alfa Aesar	Schlötter EL-KG	99.95% purity, 0.001 in
Cu	Foil	unknown	scratch in GB	>99.99%, electrolytic copper

are barely soluble.<sup>23</sup> Therefore, analytical expressions for the concentrations of red and ox in Eq. 4 will become rather complex. Therefore, we take a more phenomenological approach and describe the full current-overvoltage relation of the complex sulfur electrode using the Butler-Volmer equation with apparent limiting anodic,  $j_{la}$ , and cathodic current densities,  $j_{lc}$ , (Eq. 5) to fit current density-potential curves of the sulfur electrode. Note that in such an approach the parameters  $j_0$ ,  $j_{la}$  and  $j_{lc}$  must be considered as apparent values that describe the overall behavior of the sulfur electrode.

$$j = j_0 \cdot \frac{(e_a - e_c)}{1 + j_0 \cdot \frac{e_a}{j_{la}} - j_0 \cdot \frac{e_c}{j_{lc}}} \quad [5]$$

### Experimental

**Electrocatalyst preparation.**—For a broad variety of potential electrocatalysts (Tables I–III) the parameters  $j_0$ ,  $j_{la}$  and  $j_{lc}$  were determined.

Thin metal foils or as received materials (Al, Ni, Pt, glassy carbon, stainless steel, Co, Cu, details in Table I) were characterized. The metal foils were degreased in a commercial product (SLOTOCLEAN EL-KG, 100 g l<sup>-1</sup>, 3 V, 1 min, 50 °C, 500 rpm stirring), etched in 5 vol% H<sub>2</sub>SO<sub>4</sub> (for 30 s) and rinsed with demineralized water ( $\sigma < 2 \mu\text{S cm}^{-1}$ ) if not mentioned otherwise. The pre-treatment by degreasing and etching is marked as “treated” in the following. This pre-treatment damages (passivation, oxidation) some samples (Al, GC, SS (stainless steel), Ti, Zn and Cu substrate for Cr-electrodeposition, Al substrate for TiN coating). Such samples (marked as “sanded”) were sanded with emery paper (1000 grit) inside a glovebox (as described in section “Current density potential curves”).

The substrate for the electrodeposition and the PVD (physical vapor deposition) was nickel foil (99.6%, Schlenk Metallfolien GmbH, Germany). It was pre-treated as described above before being coated by electrodeposition or PVD.

Some materials were coated with commercially available baths or were provided by external partners (Table II, Cr samples and ITO).

**Table II. Composition and coating parameters during deposition of the screening candidates that were coated with commercially available coating procedures or externally provided samples.**

Samples	Company	Parameters
Cr (<1 wt% S)	Schlötter Hartchrom SLOTOCHROM S	Schlötter electrodeposition specifications
Cr (2–3 wt% S)	KIESOW: SAPHIR 2000	Electrodeposited at 5 A dm <sup>-2</sup> ; 50 °C
Cr (>7 wt% S)	Confidential decorative Cr(III) bath	Confidential
ITO	Kurt J. Lesker Company	Radio frequency sputtered with In <sub>2</sub> O <sub>3</sub> /SnO <sub>2</sub> 90/10 wt%—target

**Table III. Composition and working parameters during deposition of the samples that have been prepared by own electrodeposition procedures.**

Samples	Components	Amount g/l	j/A dm <sup>-2</sup>	T/°C	Coating time
Co (unstable)	CoSO <sub>4</sub>	324.80	0.50	50	10 min
	Saccharin (Na salt)	2.56			
	H <sub>3</sub> BO <sub>3</sub>	42.62			
	Butinediol	0.91			
Co	CoSO <sub>4</sub>	332.97	0.50	50	10 min
	H <sub>3</sub> BO <sub>3</sub>	42.62			
	Co-S	CoSO <sub>4</sub>			
(Na salt)	2.56				
H <sub>3</sub> BO <sub>3</sub>	42.62				
StrNi	Butinediol	0.91	3.50	65	90 s
	Thiourea	75.17			
	NiSO <sub>4</sub> ·2H <sub>2</sub> O	200.31			
	H <sub>3</sub> BO <sub>3</sub>	20.30			
Ni-S	H <sub>3</sub> PO <sub>4</sub>	94.07	2	50	5 min
	3 M™ Fluorad FC 95	20 ml l <sup>-1</sup>			
	NiSO <sub>4</sub> ·6H <sub>2</sub> O	250			
	NiCl <sub>2</sub> ·6H <sub>2</sub> O	40			
	H <sub>3</sub> BO <sub>3</sub>	35			
	Thiourea	75			

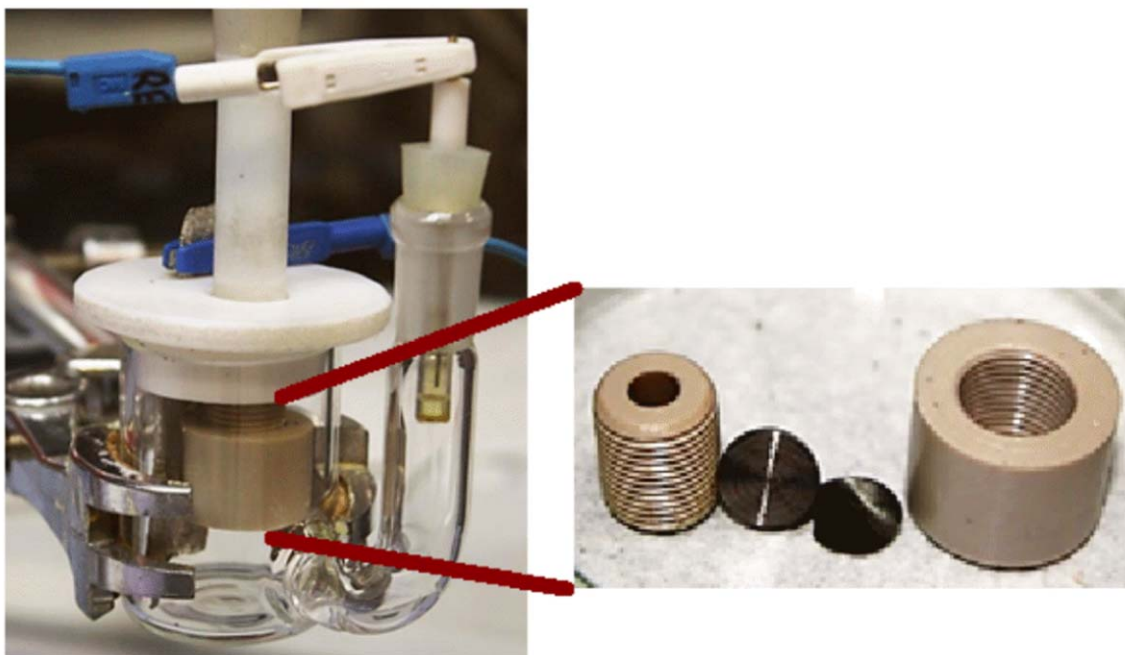


**Figure 1.** Left: Electrochemical glass cell with PTFE cover and Ag/Ag<sup>+</sup> reference electrode for the measurement of the current density potential data. Right: The PEEK tip with interchangeable sample (From right to left: Cover, which comes in contact with the electrolyte and has a well-defined hole in the bottom; Sample, which is placed inside the cover; Stainless steel current collector; The screw with internal thread for the Radiometer EDI tip and external thread for the cover. The thread is tightened until no electrolyte can float on the backside of the sample and on the current collector).

An indium tin oxide (ITO) sample was prepared by PVD. It was sputtered (Ardenne LA 440 S, Ardenne GmbH, Dresden, Germany) with radio frequency magnetron sputtering mode at room temperature (170 s, power 200 W, 80 sccm of Ar, base pressure approximately  $3 \cdot 10^{-7}$  mbar and working pressure of  $\sim 1 \cdot 10^{-3}$  mbar) on nickel (sputtering target from Kurt J. Lesker company, Clairton, USA). The resulting layer had a thickness of 300 nm.

The electrodeposited layers produced in this work (Table III) were: Co, Co-S (sulfur containing cobalt layer), structured Ni, Ni-S (sulfur containing nickel layer) and a Cr deposition. The deposited Ni-S layer had a sulfur content of approximately 10 ( $\pm 2$ ) wt%, the total sulfur content of the cathodes was quantified by a combination of total sample oxidation and subsequent SO<sub>2</sub> quantification via a nondispersive infrared sensor (CS 200, Leco Corporation, Saint Joseph, USA). Chromium was deposited in different ways, so that the resulting layers had different sulfur contents (0.8 wt% S, electrodeposition from Cr(VI); 1.5 wt% S and 7.0 wt% S both electrodeposited from Cr(III)). The sulfur content was measured by X-ray fluorescence analysis (XRF) with a Fischerscope X-ray XUV 773). Cobalt was electrodeposited from two different bath compositions (Table III) while only one of them provided stable samples.

All materials were punched in 8 or 10 mm discs.

**Current density potential curves.**—The current density-potential curves were recorded using an MPG-2 potentiostat (BioLogic, France). The control software was EC-Lab v11.01 performing potentiodynamic experiments with a sweep rate of  $50 \text{ mV s}^{-1}$ . Each material was measured at least twice with different samples, measuring at least 2000 sweeps per sample. The experiments were conducted under argon atmosphere at water and oxygen contents less than 2 ppm and 0.5 ppm, respectively, in a glovebox (Sylatech GmbH, Walzbachtal, Germany). All heat resistant materials were dried for at least 24 h at  $p < 10$  mbar and  $120 \text{ }^\circ\text{C}$  in a Memmert GmbH + Co.KG VO 200 oven (Schwabach, Germany) before being transferred into the glovebox. Thermally sensible materials (e.g. those containing elemental sulfur) were dried at  $40 \text{ }^\circ\text{C}$  for at least 48 h at  $200 \text{ mbar} < p < 500 \text{ mbar}$ .

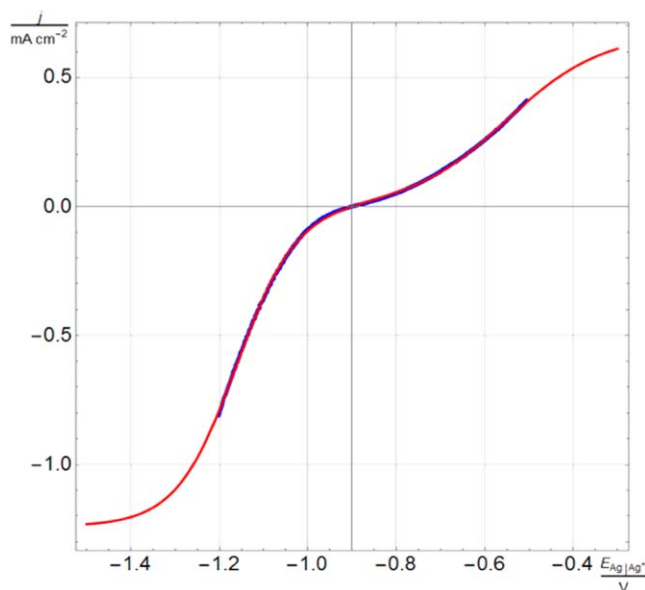


**Figure 2.** Comparison of the measured data with the Butler-Volmer fit. The current density ( $j$ )—potential (vs silver/silver nitrate reference electrode,  $U$ ) curve from the measurement (blue,  $50 \text{ mV s}^{-1}$ ,  $-0.5 \text{ V} > U > -1.2 \text{ V}$  vs  $\text{Ag}|\text{Ag}^+$ ) and the fitted curve (red, Eq. 4, fit parameters in Table IV) are similar. The displayed curves are data measured at a Co foil working electrode, 25th current density potential curve.

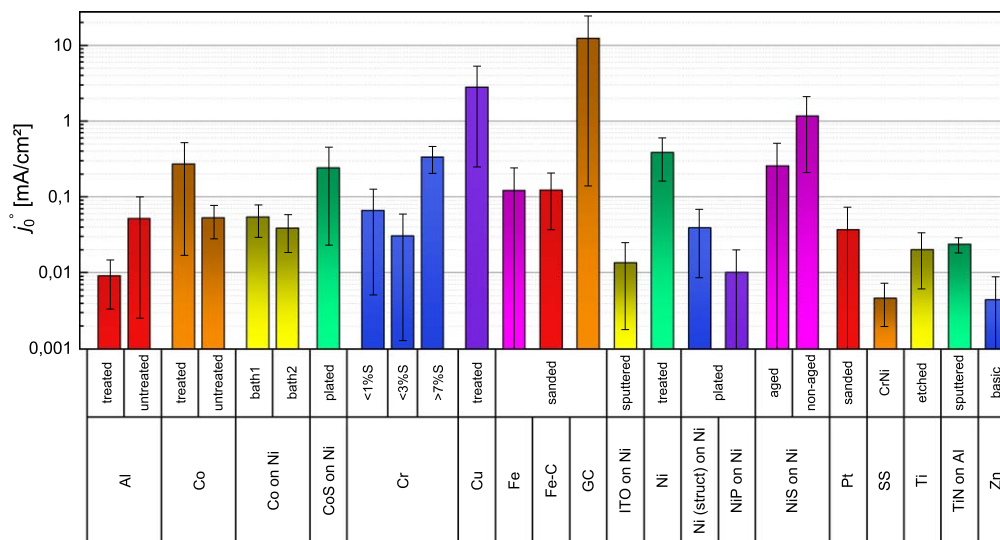
A glass cell (20 ml volume) with a side compartment for the reference electrode (RE) manufactured by H.&K. Starke GmbH (Schwäbisch Hall, Germany) was used (Fig. 1). A lab-made PTFE cover reduced electrolyte evaporation. The test discs of the materials described above were placed in the lab-made sample holder and operated as working electrodes in a three-electrode setup. The exchangeable working electrode tips (PEEK, Polyether ether ketone) were connected to a rotating disk electrode (EDI101, Radiometer,

**Table IV. Butler-Volmer fit parameters of an exchange current density curve of cobalt foil after 25 cycles (Plot with data and fit in Fig. 2).**

Parameter	Unit	Estimate	Standard Error
$j_0$	$\text{mA cm}^{-1}$	0.0263	0.0003
$b_a$	$\text{V}^{-1}$	9.27	0.063
$b_c$	$\text{V}^{-1}$	14.74	0.059
$j_{1a}$	$\text{mA cm}^{-1}$	0.671	0.008
$j_{1c}$	$\text{mA cm}^{-1}$	-1.239	0.008

Nagold, Germany) in order to remove bubbles preventing contact between electrode and electrolyte from the hole in the bottom of the tip by rotating. Thus, only a well-defined area was in contact with the electrolyte. The hole in the bottom of the tip (Fig. 1) exposed an active sample—electrode interface with an area of 0.38 or 0.36  $\text{cm}^2$  (for disks with an outer diameter of 10 mm). A commercial electrode holder with 0.28  $\text{cm}^2$  active surface was used with electrode disks with an outer diameter of 8 mm (E11.OGL.001 EDI TIP, BellTech GmbH, Wesel, Germany).

The electrolyte was prepared by mixing 50:50 vol% DME:DOL (DME 99.5%, Sigma-Aldrich; DOL 99.8% Sigma-Aldrich) as

**Figure 3.** The different  $j_0^*$  from the current density potential curves on a logarithmical scale. Al, Co and Ni-S were measured and evaluated after different pretreatments, Co and Cr were differently electrodeposited before the measurement.**Table V. Examined materials and coatings, their apparent exchange current density ( $j_0^*$ ) and their suitability as electrocatalytic material in lithium sulfur batteries. Abbreviations: GC: Glassy carbon, ITO: Indium tin oxide SS: Stainless steel, StrNi: Structured nickel electrodeposition,<sup>25</sup> p: passivation, n: not stable, x: not suitable, ✓: low suitability, ✓✓: high suitability.**

Material	$j_0^*$ in $\text{mA/cm}^2$	Stability	Suitability	Comment
Al	0.025	p	x	Passivation after 2–10 $j$ - $U$ -curves
Co metal foil	0.121	✓✓	✓✓	high $j_0^*$ , stable >5000 cycles
Co	0.046	✓✓	✓✓	Electrodeposited sample performs almost like foil, high $j_0^*$ , stable >5000 cycles
Co-S	non-reproducible	n	x	Delamination of the coating
Cr, 0.8 wt% S	0.067	n	X	High fluctuation of $j_0^*$ , surface becomes matt during measurement
Cr, 1.5 wt% S	0.031	✓	x	High fluctuation of $j_0^*$ , decreasing during measurement
Cr, 7.0 wt% S	0.337	✓	✓	$j_0^*$ decreasing during measurement
Cu	2.805	n	x	Black CuS and CuS <sub>2</sub> products (XRD)
Fe	0.122	n	x	Poorly reproducible
Fe-C	0.123	n	x	
GC	non-reproducible	n	x	High fluctuation of $j_0^*$ , decreasing during measurement
ITO	0.046	✓	x	Expensive, poorly reproducible
Ni	0.622	n	✓	Higher $j_0^*$
Ni-Co-S	non-reproducible	n	x	Delamination of the coating
Ni-S	0.817	n	x	Low $j_0^*$ after some month of storage in Ar, cracks in contact with electrolyte
Pt	0.020	n	x	Expensive, no benefits, chemical reaction with polysulfides
SS	0.052	n	x	Low $j_0^*$ increasing during measurement
StrNi	0.039	n	x	$j_0^*$ decreasing during measurement, electrochemically unstable
Ti	non-reproducible	p	x	Passivation after ca. 25 cycles
TiN	0.024	✓	x	Well reproducible, low $j_0^*$ , chemically stable
Zn	non-reproducible	p	x	Ohmic behavior, passivating

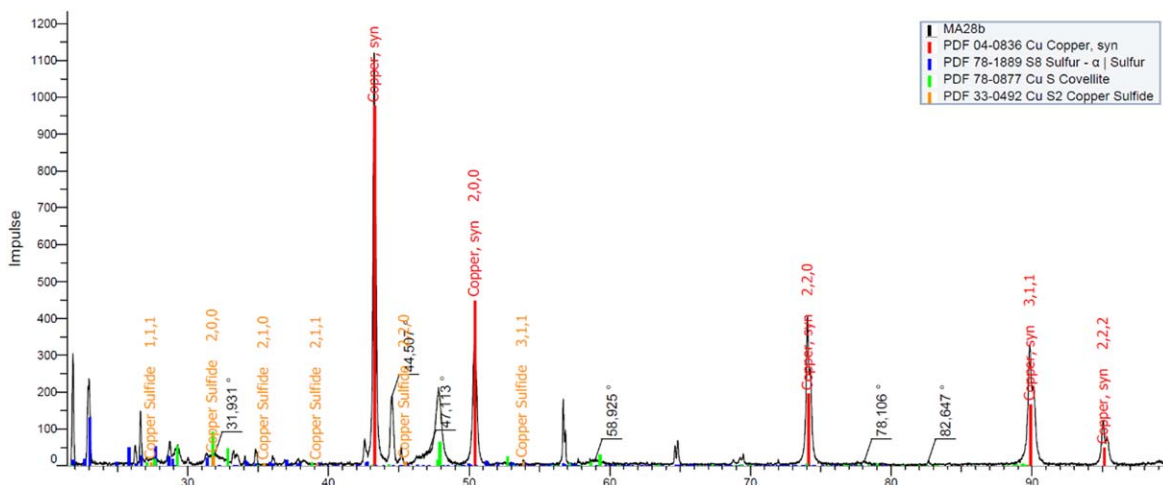


**Figure 4.** XRD pattern of the rough grey substance emerging after the current density potential measurement of copper. CuS Covellite and CuS<sub>2</sub> are the reaction products with the polysulfide electrolyte after some cycles of the measurement.

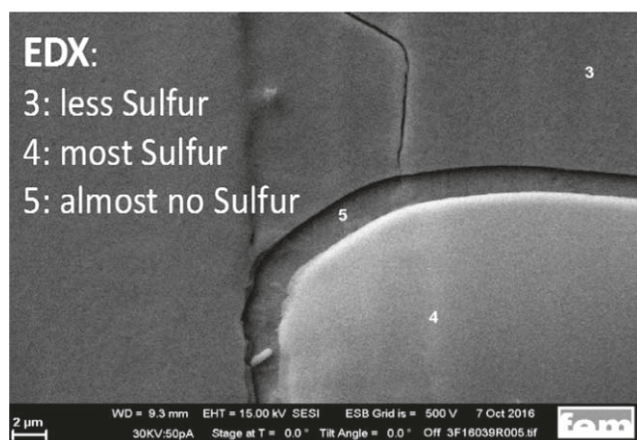
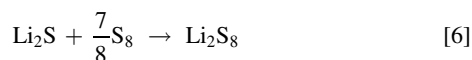


**Figure 5.** SEM image of a Ni-S sample electrodeposited from a thiourea-containing nickel bath with cracks that form after storage in polysulfide electrolyte at open circuit potential for 13 d. The further reaction with sulfur in the polysulfide containing electrolyte changes the cell parameters of the crystal which leads to cracks and partly delamination.

solvent, 1 mol l<sup>-1</sup> bis-(trifluoromethane)-sulfonimide lithium salt (LiTFSI, 99.95%, Sigma-Aldrich) as supporting electrolyte and 0.75 mol l<sup>-1</sup> lithium nitrate (LiNO<sub>3</sub>, 99.99%, Alfa-Aesar) as SEI (solid electrolyte interphase) forming agent. Then, Li<sub>2</sub>S (99.98%, Sigma Aldrich) and S<sub>8</sub> (99.998%, Sigma Aldrich) were added stoichiometrically and stirred for at least three days to form an electrolyte containing formally 0.125 mol l<sup>-1</sup> Li<sub>2</sub>S<sub>8</sub> (Eq. 6). Due to various disproportion reactions, other polysulfides (Li<sub>2</sub>S<sub>x</sub>, 2 ≤ x < 8) are formed.<sup>24</sup>



A lithium sheet of ca. 5 cm × 2 cm × 1.5 mm (99.9% metals basis, Alfa Aesar) was used as counter electrode (CE). The lithium sheet could be used several times. Before usage, the surface was scratched with a spatula until the shining metallic visual appearance was restored. Two different reference electrodes (RE) were set up. An Ag|Ag<sup>+</sup> RE (RE-7s by ALS Co., Ltd., Tokyo, Japan) was utilized. In order to prevent the silver to react with sulfur diffusing into the reference electrode, a solution of 1 mol l<sup>-1</sup> LiTFSI in 1:1 vol % DME:DOL containing salt bridge separated the polysulfide and the reference electrolyte by two CoralPor® 1000 glass frits (pore size ~ 7.8 nm, Schott, Duryea, USA). In later experiments a platinum

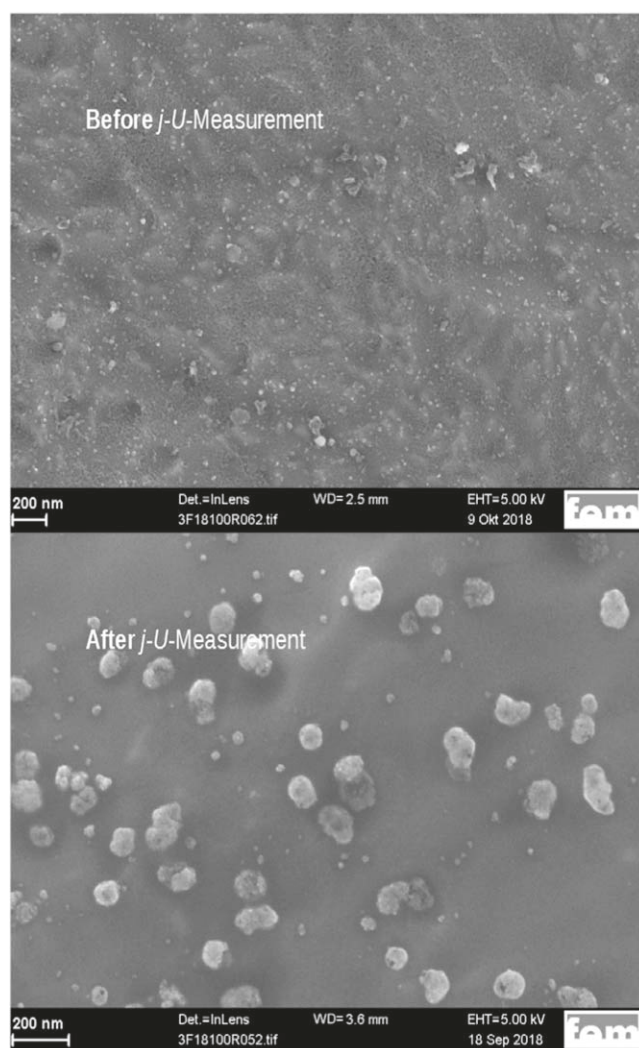


**Figure 6.** The surface of two titanium samples, before (top) and after (bottom) 2000 cycles of the *j-U*-measurement.

quasi RE was employed for two reasons. First, it can be placed directly into the polysulfide electrolyte and second, the glass frits of the RE-7s clogged with silver sulfide lowering their conductivity.

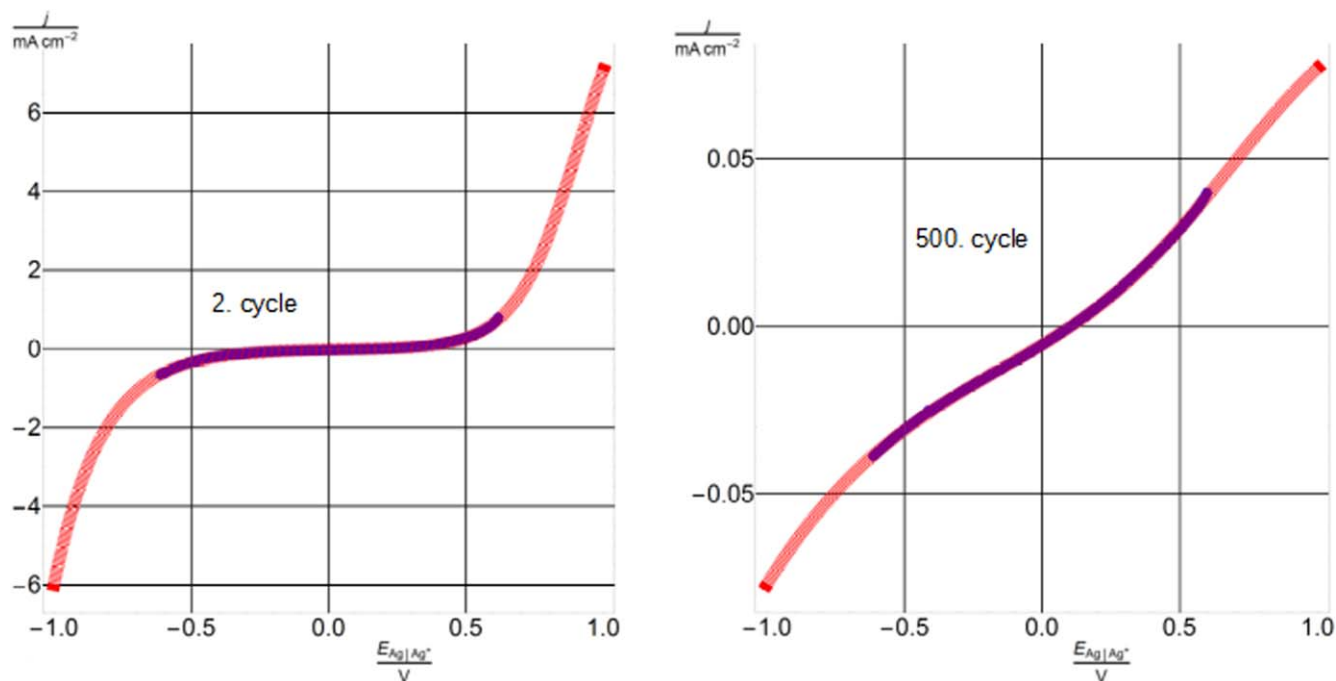


**Figure 7.** Second cycle (left) and 500th cycle (right) of aluminum's current density potential data (blue) and fits (red). In the beginning of the measurement, a Butler-Volmer characteristic curve is recorded. After a few cycles, the ohmic resistance rises and the curve becomes linear.

For both REs the voltammetry curves were reproducible with a 0.85 V shift of the potential axis.

The reported  $j_0^*$  values are the result of a Butler-Volmer fit (Wolfram Mathematica version 11.1.1.0) with consideration of concentration polarization, Eq. 5. The source code is attached as supplementary file (S.1 available online at [stacks.iop.org/JES/167/166520/mmedia](https://stacks.iop.org/JES/167/166520/mmedia)).

**Further analysis.**—The XRD analyses were performed with a Bruker AXS D8 Discover with General Area Detector Diffraction System configuration. The Cu-K $\alpha$  ray diffraction was evaluated with the software DIFFRAC.EVA 4.2 and the database ICDD-PDF-2. SEM images were recorded with a Zeiss Auriga 60. Sulfur content analysis was performed by X-ray fluorescence analysis with a Fischerscope X-ray XUV 773.

## Results and Discussion

Figure 2 compares measured data and the fitted curve for cobalt (representative for the evaluation procedure). Table IV provides the results of this exemplary fit. Both Fig. 2 and Table IV demonstrate that experimental data and the used Butler-Volmer-fit are in good accordance. The apparent exchange current density is our main parameter for assessing the electrocatalytic activity of the different materials. A comparison of the different material's  $j_0^*$  is visualized in Fig. 3 and Table V. The data displayed are average values of the  $j_0^*$  evaluated from the 2nd cycles of  $j$ - $U$ -measurements of each material. The error bars in Fig. 3 represent the  $j_0^*$  standard deviation from the individual measurements of a material. Another aspect of the suitability of the electrocatalyst is the reproducibility of the  $j$ - $U$ -curves. The reproducibility of the experiments on the same material can be judged from the error bars in Fig. 3, larger error bars correspond to a worse reproducibility than smaller bars.

**Unstable materials.**—Some of the investigated materials that are at first glance promising candidates as electrocatalyst for the polysulfide reactions due to the high  $j_0^*$  values do not provide a stable performance upon cycling. The least reproducible materials

with the largest errors of  $j_0^*$  are GC, Pt, Fe, Zn, NiP, Cr with low S-contents and aged NiS on Ni and untreated Al. We consider a standard error as a criterion for the unsuitability of a material as catalyst for the Li-S cathode. In addition to the current density potential curves, XRD data, SEM images and photo images were taken to investigate the materials' stability.

For some materials, a change of the surface during the measurement is already visible with the bare eye. Cu is the material with the highest  $j_0^* = 2.81 \text{ mA cm}^{-2}$ , but suffers from low stability in contact with polysulfides and forms a black, brittle substance. The black product was identified as a mixture of CuS and Cu $_2$ S $_2$  by XRD (Fig. 4). Obviously, the high  $j_0^*$  originates from this corrosion mechanism and not from a reversible reaction of polysulfide and Cu can be discarded as a potential electrocatalyst for reaction 1.

Similarly, the surface of Ni ( $j_0^* = 0.841 \text{ mA cm}^{-2}$ ) showed clearly visible changes during the voltammetry measurements. After rinsing with DOL, a black circle remains on the surface (Fig. S.2) and the rest of the active surface becomes rough and loses its shiny metallic appearance. The black spot probably corresponds to the formation of NiS, Ni $_2$ S, or Ni $_2$ S $_3$  with presence of Li $_2$ S $_8$ . The respective reaction enthalpies are negative<sup>26–28</sup> (S.3,<sup>26,27,29</sup>  $\Delta H = -653 \text{ kJ mol}^{-1}$ ). In an ex situ XRD measurement, a lithium nickel oxide (S.4, Li $_{0.524}$ Ni $_{1.476}$ O $_2$ ) was found which was probably formed when the NiS was in contact with the ambient air during sample transfer. The reaction enthalpy of the reaction of NiS in O $_2$  containing atmosphere towards LiNiO $_2$  is negative as well (S.5<sup>26,27,29</sup>).

Pt ( $j_0^* = 0.020 \text{ mA cm}^{-2}$ ) unveils a low  $j_0^*$  which increases strongly during the first 400 cycles. The surface changes from shiny metallic to dark grey as in the case of Ni.

Fe (becomes brown and rough;  $j_0^* = 0.122 \text{ mA cm}^{-2}$ ) and carbon steel (becomes brown-rough and nuclei emerge;  $j_0^* = 0.123 \text{ mA cm}^{-2}$ ) change visibly. The surfaces become more opaque and lose the metallic gleam. Additionally, the  $j_0^*$  decreases within the first 250  $j$ - $U$ -cycles.

A structured electrodeposited Ni electrode was expected to exhibit high  $j_0^*$  due to the increased surface area. However, the  $j_0^*$

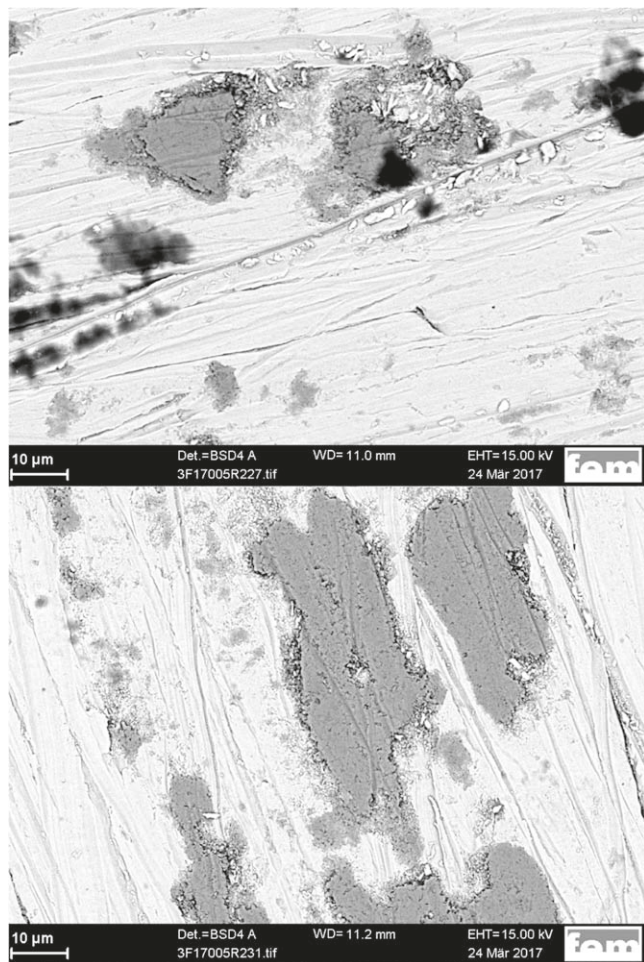


**Figure 8.** SEM images of two Cobalt foil samples, one before (top) and one after (bottom) a measurement with 5000 cycles of current density potential curves at  $50 \text{ mV s}^{-1}$  from  $-0.5 \text{ V}$  to  $-1.5 \text{ V}$  vs  $\text{Ag|Ag}^+$  reference electrode. The almost same structure is evidence for the stability of cobalt under the experimental conditions.

is lower than expected ( $0.039 \text{ mA cm}^{-2}$ ) and roughly halves during the first 500 cycles of a  $j$ - $U$ -measurement.

The  $j_0^*$  of an electrochemical Ni-S codeposition<sup>30,31</sup> ( $j_0^* = 0.817 \text{ mA cm}^{-2}$ ) strongly decreases when stored in Ar for five months and after 13 d in the polysulfide electrolyte without electrochemical measurement the Ni-S layer cracks and partly delaminates (Fig. 5).

After the  $j$ - $U$ -measurements, the electrodeposited Ni-Co-S and Co-S coatings are unstable in the presence of polysulfides, delaminated and lost contact with the substrate.

**Passivating materials and irreproducible  $j$ - $U$ -curves.**—The  $j_0^*$  of GC varies strongly in similar experiments. Thus, it does not seem to be a suitable electrocatalytic material. The  $j$ - $U$ -measurements and the resulting  $j_0^*$  of ITO were not reproducible probably due to slightly different stoichiometries of the samples as confirmed with XRF.

The  $j_0^*$  values of some materials decrease after few  $j$ - $U$ -cycles and the shapes of the curves become almost linear. Such ohmic behavior can be interpreted as increasing passivation of the electrode material. This phenomenon was observed for Zn with an ohmic linear curve from the second  $j$ - $U$ -cycle. The surface of Ti samples changes from shiny metallic silver to a rough grey and SEM images (Fig. 6) reveal significant morphology changes during the  $j$ - $U$ -measurements which become irreproducible and linear within 25 cycles. Al passivates within the first 5 cycles with increasing ohmic

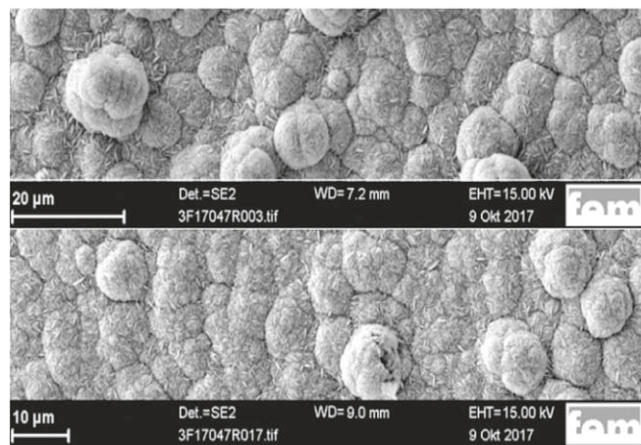


**Figure 9.** SEM images of two electrodeposited cobalt layer samples before (top) and after 5000 current density potential measurement cycles at  $50 \text{ mV s}^{-1}$  from  $-0.1 \text{ V}$  to  $-1.5 \text{ V}$  vs  $\text{Ag|Ag}^+$  reference electrode.

behavior (Figs. 7 and S.6) and a low  $j_0^* = 0.025 \text{ mA cm}^{-2}$  in the 2nd cycle. A passivation mechanism involving a sulfide-containing non-conducting surface layer is most probable for Zn, Ti and Al.

The  $j_0^*$  of Cr and Ni containing stainless steel samples (1.4305) are initially low but increase after some cycles, probably because the passivating oxide layer is partly dissolved.<sup>32,33</sup> Steel samples without further alloying elements indicate a surface change and a shift of the current density potential curve after a few cycles. Therefore, the materials containing iron are not considered suitable in the sulfur half-cell.

**Stable materials.**—For the electrodeposited Cr coatings higher sulfur content has a negative impact on the reproducibility of the  $j_0^*$ .

Co metal foil has an average  $j_0^*$  in the order of  $0.121 \text{ mA cm}^{-2}$  and the surface of the Co foil remains unaltered after the potentiodynamic measurements (Fig. 8). Hence, Co is considered electrochemically stable and several samples with electrodeposited Co catalyst were tested. One Co electrodeposition bath was operated with further additives (saccharin and 1,4-butyndiol; Table III), another Co plating was performed without additives ( $\text{CoSO}_4$  and  $\text{H}_3\text{BO}_3$ ) to realize a pure Co coating. The Co samples electrodeposited with 1,4-butyndiol and saccharine delaminated during electrodeposition, drying or during the measurement. In another bath, thiourea (Sigma Aldrich, >99.0%) was added to co-deposit S, resulting in a Co-S coating with around 10 wt% S which cracked and delaminated during the  $j$ - $U$ -measurement. The plating without the additives  $\text{CoSO}_4$  and  $\text{H}_3\text{BO}_3$  was stable, yielding samples with highly reproducible  $j_0^* = 0.040 \text{ mA cm}^{-2}$  and a good  $j$ - $U$ -cycling stability after 5000 cycles (Fig. 9).

An electrochemical cobalt deposition was used to be able to deposit active particles on an electrically conductive substrate and the electrochemical performance was proven to be like Co foil.

Since Ti and Al passivate (see above), a TiN sputtered sample (on Al foil) reveals a reproducibly low  $j_0^* = 0.022 \text{ mA cm}^{-2}$ . The SEM images reveal that the surface morphology remains unchanged (Fig. 10) which is in accordance with the  $j$ - $U$ -measurement results with Butler-Volmer characteristics until the 5000th cycle.

## Conclusions

This screening of current density potential curves for different materials has been performed to determine an electrochemically and chemically stable electrocatalyst for the sulfur redox reactions in Li-S batteries.

In order to evaluate the electrocatalytic activity of the examined materials, a Wolfram Mathematica script (S.1) was written to

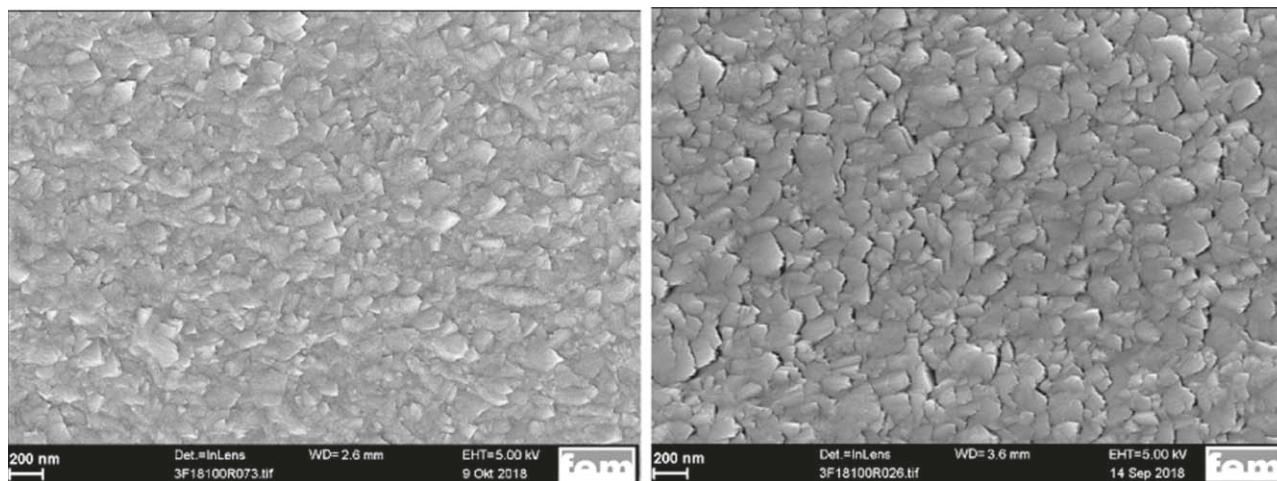


**Figure 10.** SEM images of two sputtered TiN coating samples, one before (left) and one after (right) 2000 cycles of current density potential curves at  $50 \text{ mV s}^{-1}$  from  $0.6 \text{ V}$  to  $-0.6 \text{ V}$  vs Pt wire.

perform a Butler-Volmer fit with a much higher precision than the common Tafel evaluation since it uses the complete set of measured data and does not leave out the data points near the equilibrium potential. The fit model takes into consideration different anodic and cathodic limiting currents due to the complex polysulfide electrochemistry. The diffusion limitation is different for different polysulfide chain lengths while the rate limiting reaction steps might vary. The accuracy of the fits for  $j_0^*$  was around 1%–2%, depending on the sample material.

The highest  $j_0^*$  are observed for materials that undergo irreversible chemical or electrochemical reactions in a polysulfide environment at the operating potentials of the sulfur electrode (and therefore are unsuitable for the use as an electrode material). Various  $j_0^*$  were found amongst the stable S electrocatalysis candidates, although not as high as expected as in other electrocatalysis fields such as the hydrogen ( $10^{-10} < j_0 / \text{A cm}^{-2} < 10^{-3}$ ).<sup>14,34</sup>

Due to excellent long-term stability and its relatively high  $j_0^*$  ( $0.121 \text{ mA cm}^{-2}$ ), cobalt was electrochemically plated with two different electrolytes to prepare an economic electrocatalyst. The samples electroplated without the additives 1,4-butyne diol and saccharine provided the same stability of Co foil ( $0.040 \text{ mA cm}^{-2}$ ).

In conclusion, cobalt seems to be a good electrocatalyst for the sulfur reactions. Materials with a higher  $j_0^*$  ( $>0.040 \text{ mA cm}^{-2}$ ) did not meet the stability criteria evaluated from optical observation, SEM images and XRD patterns and from the increase or decrease of  $j_0^*$  after some  $j$ - $U$ -cycles.

With this procedure an economical use of Co can be realized at the S-electrode to potentially improve the cycle-life, cycle rate and as a result the energy efficiency of Li-S batteries. This approach could bolster the Li-S battery on its way towards commercialization and should be pursued.

Future work will be directed towards the electrocatalytic efficiency of Co and its stability in a lab-scale Li-S battery. With a better understanding of the mechanism, simulations could predict the suitability of a material in a manner that only specific materials need to be tested in the laboratory.<sup>35,36</sup> A DFT simulation could aid discover electrocatalytically surfaces to establish active structures to further ameliorate the material's effectiveness.<sup>37,38</sup>

### Acknowledgments

We thank the German Federal Ministry of Economic Affairs and Energy for funding this research work under grad. no. BMWi 03ET6084. We thank Lisa Bükler, Mario Kurniawan, Martin Leimbach and Violeta Gruia for providing samples for the exchange

current density measurements screening. Further thanks go to KIESOW Dr. Brinkmann GmbH & Co KG for providing a set of industrially coated samples.

### ORCID

M. J. Ante  <https://orcid.org/0000-0002-2273-9733>

A. Bund  <https://orcid.org/0000-0001-9837-2408>

### References

1. L. Zeng, Y. Jiang, J. Xu, M. Wang, W. Li, and Y. Yu, *Nanoscale*, **7**, 10940 (2015).
2. X. Ji and L. F. Nazar, *J. Mater. Chem.*, **20**, 9821 (2010).
3. D. N. Fronczek and W. G. Bessler, *J. Power Sources*, **244**, 183 (2013).
4. Z. Li, Y. Huang, L. Yuan, Z. Hao, and Y. Huang, *Carbon*, **92**, 41 (2015).
5. D. Aurbach, E. Pollak, R. Elazari, G. Salitra, C. S. Kelley, and J. Affinito, *J. Electrochem. Soc.*, **156**, A694 (2009).
6. B. D. Katz, M.-Y. Chu, L. C. Dejonghe, and S. J. Visco, (2001), 1–21 ([https://patentscope.wipo.int/search/docs2/iasr/WO2001057943/pdf/bAGVjn5cWS5F5RS0Lo\\_P7ioO9fHyb-0I09I2i9NrZz2mlDBLHnCh25V48bfsHvKLT06fZsOCLKbB57FNx0pfK4Gc-KkwVJG999bHMUGW2QUlrkzEmy-KUluR9Ue9jAz5?filename=US2001002909-IASR.pdf&psAuth=-HT-TpJEsARAPj4VA3ADaQYmIv\\_hpt7qaBs-th3AGoQ](https://patentscope.wipo.int/search/docs2/iasr/WO2001057943/pdf/bAGVjn5cWS5F5RS0Lo_P7ioO9fHyb-0I09I2i9NrZz2mlDBLHnCh25V48bfsHvKLT06fZsOCLKbB57FNx0pfK4Gc-KkwVJG999bHMUGW2QUlrkzEmy-KUluR9Ue9jAz5?filename=US2001002909-IASR.pdf&psAuth=-HT-TpJEsARAPj4VA3ADaQYmIv_hpt7qaBs-th3AGoQ)) US-patent WO 2001057943 A1.
7. B. Zhang, C. Lai, Z. Zhou, and X. P. Gao, *Electrochim. Acta*, **54**, 3708 (2009).
8. S. S. Zhang, *J. Power Sources*, **231**, 153 (2013).
9. X. Han et al., *Nano Energy*, **2**, 1197 (2013).
10. X. Wang, Z. Wang, and L. Chen, *J. Power Sources*, **242**, 65 (2013).
11. C. Zhao, C. Shen, F. Xin, Z. Sun, and W. Han, *Mater. Lett.*, **137**, 52 (2014).
12. C. Shuangqiang et al., *J. Mater. Chem. A*, **2**, 16199 (2014).
13. N. Mansor et al., *Electrochim. Acta*, **222**, 44 (2016).
14. P. Quaino, F. Juarez, E. Santos, and W. Schmickler, *Beilstein J. Nanotechnol.*, **5**, 846 (2014).
15. B. Hariprakash, P. Bera, S. K. Martha, S. A. Gaffoor, M. S. Hegde, and A. K. Shukla, *Electrochim. Solid-State Lett.*, **4**, A23 (2001).
16. J. Zhu, P. Xiao, H. Li, and S. A. C. Carabineiro, *ACS Appl. Mater. Interfaces*, **6**, 16449 (2014).
17. B. C. Gates, *J. Catal.*, **328**, 72 (2015).
18. T. Xu, H. Huang, W. Luan, Y. Qi, and S.-T. Tu, *Sens. Actuators B Chem.*, **133**, 70 (2008).
19. H. Wang, Q. Guan, J. Li, and T. Wang, *Catal. Today*, **236**, 121 (2014).
20. C. H. Hamann and W. Vielstich, *Elektrochemie* (Wiley-VCH-Verlag GmbH & Co. KGaA) 4. vollständig überarbeitete und aktualisierte Auflage. (Weinheim) p. 662 (2005).
21. A. J. Bard and L. R. Faulkner, *Electrochemical Methods: Fundamentals and Applications* (Wiley, New York) 2nd ed., p. 833 (2001).
22. M. Vijayakumar et al., *Phys. Chem. Chem. Phys.*, **16**, 10923 (2014).
23. F. Y. Fan, W. H. Woodford, Z. Li, N. Baram, K. C. Smith, A. Helal, G. H. McKinley, W. C. Carter, and Y. M. Chiang, *Nano Lett.*, **14**, 2210 (2014).
24. L. Wang, T. Zhang, S. Yang, F. Cheng, J. Liang, and J. Chen, *J. Energy Chem.*, **22**, 72 (2013).
25. H. Willing, *Elektrolyt-Rezepturen für Strukturnickel und Nickel-Phosphor-Schichten* (Forschungsinstitut Edelmetalle + Metallchemie (fem), Schwäbisch Gmünd) (2016).
26. A. Jain et al., *APL Mater.*, **1**, 011002 (2013).
27. K. Persson et al., *Mater. Proj.* (2020), (<https://materialsproject.org/dashboard>).
28. W. D. Richards, L. J. Miara, Y. Wang, J. C. Kim, and G. Ceder, *Chem. Mater.*, **28**, 266 (2016).

29. A. Jain, G. Hautier, S. P. Ong, C. J. Moore, C. C. Fischer, K. A. Persson, and G. Ceder, *Phys. Rev. B*, **84**, 045115 (2011).
30. S. Sörgel, O. Kesten, A. Bock, and T. Sörgel, *Meet. Abstr.*, **MA2016-01**, 250 (2016).
31. S. Sörgel, *Ni/S-Abscheidung auf Ni-Folien* (FEM—Forschungsinstitut Edelmetall und Metallchemie, Schwäbisch Gmünd) p. 6,10 (2015).
32. A. Bhattacharya and P. M. Singh, *J. Fail. Anal. Prev.*, **7**, 371 (2007).
33. C. F. Dong, K. Xiao, X. G. Li, and Y. F. Cheng, *J. Mater. Eng. Perform.*, **20**, 1631 (2011).
34. Y. Zheng, Y. Jiao, Y. Zhu, L. H. Li, Y. Han, Y. Chen, A. Du, M. Jaroniec, and S. Z. Qiao, *Nat. Commun.*, **5**, 1 (2014).
35. M. Andersson, T. Bligaard, A. Kustov, K. Larsen, J. Greeley, T. Johannessen, C. Christensen, and J. Nørskov, *J. Catal.*, **239**, 501 (2006).
36. Y. Yang, Z. Liu, R. Cheng, X. He, and B. Liu, *Organometallics*, **33**, 2599 (2014).
37. J. J. Lukkien, J. P. L. Segers, P. A. J. Hilbers, R. J. Gelten, and A. P. J. Jansen, *Phys. Rev. E*, **58**, 2598 (1998).
38. H. Over, *Chem. Rev.*, **112**, 3356 (2012).